HOG ACTIVE APPEARANCE MODELS

Epameinondas Antonakos[⋆]*, Joan Alabort-i-Medina*[⋆]*, Georgios Tzimiropoulos*[†⋆]*, Stefanos Zafeiriou*[⋆]

[⋆]Imperial College London, Department of Computing, U.K.
[†]University of Lincoln, School of Computer Science, U.K.

ABSTRACT

We propose the combination of dense Histogram of Oriented Gradients (HOG) features with Active Appearance Models (AAMs). We employ the efficient Inverse Compositional optimization technique and show results for the task of face fitting. By taking advantage of the descriptive characteristics of HOG features, we build robust and accurate AAMs that generalize well to unseen faces with illumination, identity, pose and occlusion variations. Our experiments on challenging in-the-wild databases show that HOG AAMs significantly outperfrom current state-of-the-art results of discriminative methods trained on larger databases.

Index Terms— Active Appearance Models, Histogram of Oriented Gradients, Inverse Compositional optizimation

1. INTRODUCTION

Active Appearance Models (AAMs) are generative parametric deformable statistical models of the shape and appearance variation of an object that are widely used in various tasks of Human-Computer Interaction and Image and Video Processing. They have been used in numerous applications such as face fitting, facial expressions recognition and medical imaging. They were initially proposed in [1] and they are descendants of Active Contour Models [2] and Active Shape Models [3]. The fitting process of an AAM aims to bring a test image into registration with a reference template, even if the test image is a deformed instance of the template. The most common choise for fitting an AAM is the Inverse Compositional (IC) optimization techique [4, 5, 6], though other methodologies have been used, such as regression [1, 7]. IC is a non-linear gradient descent optimization algorithm that attempts to minimize the discrepancy between a warped input image and a parametric model instance with respect to the shape and appearance parameters.

Since IC is a gradient descent method, the alignment is sensitive to initialization and to large appearance variations in terms of illumination, expressions, occlusion and identity. Especially, in the case of intensities-based AAMs with the Project-Out IC algorithm [4], the model is incapable of adequately generalizing in order to be robust to outliers. This is the main reason why AAMs have been criticized of being able to perform well only in person specific applications and not generic ones. In this paper, we show that the combination of the IC framework with a powerful and descriptive features descriptor results in a generic deformable model with remarkable performance.

The concept of dense feature-based image representation is also adopted in [8], where the authors use correspondences between densely computed SIFT descriptors. However it is applied on scene alignment and face recognition and not on deformable models fitting. There are several attempts in recent bibliography to build a feature-based AAM framework. The authors in [9] use novel features based on the orientations of gradients to represent edge structure within a regression framework. Similar features are employed in [6] to create a robust similarity optimization criterion. In [10] a combination of grayscale intensities, hue channel and edge magnitude is used to build the appearance model. Moreover, the work in [11] applies the IC optimization algorithm in the Fourier domain using Gabor responses. In [12] a new appearance representation is introduced for AAMs by combining Gabor wavelet and Local Binary Pattern descriptor. The authors in [13] employ Gabor magnitude features summed over either orientations or scales or both to build an appearance model. Similarly, the authors in [14] model the characteristic functions of Gabor magnitude and phase by using lognormal and Gaussian density functions respectively and utilize the mean of the characteristics over orientations and scales.

In this paper, we employ densely-sampled Histogram of Oriented Gradients (HOG) features [15] to train the AAM appearance model. To the best of our knowledge, this is the first time that a *generic* feature-based AAM is developped using dense HOGs. We perform cross-database experiments on in-the-wild images using two IC algorithms: Alternating IC (AIC) [5] and Project-Out IC (POIC) [4]. Finally, we show that our HOG AAMs greatly outperform state-of-the-art methods in facial alignment, which are discriminatively trained on much more data than our approach.

2. HISTOGRAMS OF ORIENTED GRADIENTS

We extract *dense* HOG descriptors at each pixel of an image, based on the method introduced in [15]. This means that given an input image of size $H \times W$, the densely-sampled multichannel features image has size $H \times W \times D$. Let us denote the HOG features extraction function as $\mathcal{H}$ and an input image in vectorial form as $\mathbf{t}$ with length L_T. Then the HOG image in vectorial form is

$$\mathbf{h} = \mathcal{H}(\mathbf{t}) \tag{1}$$

where $\mathcal{H} : \mathbb{R}^{L_T \times 1} \longrightarrow \mathbb{R}^{L_T D \times 1}$. The HOG extraction function clusters gradient orientations in different bins for localized subwindows of the input image. Specifically, we first compute the image gradient and in the case of an RGB image, we keep the gradient with the largest norm between the gradients of the three channels. For each pixel of the image, we use two spatial neighbourhoods: cells and blocks. A *cell* is a small rectangular sub-window of size N_{cell} pixels in height and width, from which we create a histogram of the gradient orientations weighted by the gradient magnitude of each pixel. This orientation binning procedure reveals the non-linear nature of the HOG descriptors. Each histogram has N_{bins} and we apply trilinear interpolation between the votes of neighbouring bin

The work of Epameinondas Antonakos and Stefanos Zafeiriou was partially funded by the EPSRC project EP/J017787/1 (4D-FAB). The work of Joan Alabort-i-Medina was funded by the Qualcomm Innovation Fellowship and by a European DTA from Imperial College London.

(a) Original image (b) $N_{cell} = 8$, $N_{block} = 2$ (c) $N_{cell} = 4$, $N_{block} = 2$ (d) $N_{cell} = 8$, $N_{block} = 1$ (e) $N_{cell} = 4$, $N_{block} = 1$

Fig. 1. Example of dense HOG features. N_{cell} denotes the cell height and width in pixels and N_{block} denotes the number of cells that consist a block. Thus, *(b)* and *(c)* have $D = 36$ channels whereas *(d)* and *(f)* have $D = 9$ channels. We visualize the sum over all the D channels.

centres with respect to orientation and position. A *block* is a larger spatial neighbourhood that consists of $N_{block} \times N_{block}$ cells. After applying contrast normalization at each block, the final descriptor vector at each image pixel is constructed by concatenating the histograms of the cells, thus it has length $D = N_{bins} N_{block}^2$.

The local contrast normalization adopted at each block is essential as it makes the features image invariant to illumination and foreground-background intense differences. Thus, HOG features have great advantages, such as invariance to geometric and photometric variations, which are important for building robust generic deformable models. We altered the code provided by [16] in order to extract dense HOG features. We use $N_{bins} = 9$ histogram bins and experiment with the cell size ($N_{cell} \in \{4, 8\}$) and the block normalization ($N_{block} \in \{1, 2\}$). Figure 1 shows indicative HOG images by summing over all their channels.

3. HOG ACTIVE APPEARANCE MODELS

3.1. Training

Let us denote a shape instance of L_S landmark points as $\mathbf{s} = [x_1, y_1, \ldots, x_{L_S}, y_{L_S}]^T$. The *shape model* is constructed by aligning a set of training shapes $\{\mathbf{s}_i\}$ using Genaralized Procrustes Analysis and applying Principal Component Analysis (PCA) on the aligned shapes to end up with an orthonormal basis of N_S eigenvectors $\mathbf{U}_S \in \mathcal{R}^{2L_S \times N_S}$ and the mean shape $\bar{\mathbf{s}}$. The first four eigenshapes correspond to the similarity transform parameters that control the global rotation, scaling and translation. A shape instance is generated as $\mathbf{s_p} = \bar{\mathbf{s}} + \mathbf{U}_S \mathbf{p}$, where $\mathbf{p}$ is the $N_S \times 1$ vector of shape parameters. The *motion model* consists of the warp function $\mathcal{W}(\mathbf{p})$, which maps the points within a source shape to their corresponding coordinates in a target shape. We employ the Piecewise Affine Warp, which performs the mapping based on the barycentric coordinates of the corresponding triangles between the two shapes that are extracted using Delaunay Triangulation.

Given a set of training annotated images $\{\mathbf{t}_i\}$, we compute their HOG features $\{\mathbf{h}_i\}$ (Eq. 1) and warp them into the mean shape $\bar{\mathbf{s}}$, ending up with a set of aligned vectors. Each vector has length L_A, i.e. the number of pixels that lay inside the mean shape. Then we apply PCA to find an appearance subspace $\mathbf{U}_A \in \mathbb{R}^{L_A \times N_A}$ of N_A eigentextures and the mean appearance vector $\bar{\mathbf{a}}$. Synthesis is achieved through linear combination of the eigentextures as $\mathbf{a_\lambda} = \bar{\mathbf{a}} + \mathbf{U}_A \boldsymbol{\lambda}$, where $\boldsymbol{\lambda}$ is the $N_A \times 1$ appearance parameters vector.

3.2. Inverse Compositional Optimization

The aim of AAM fitting is to minimize the ℓ_2-norm between an input vectorized HOG image $\mathbf{h}$ and the HOG appearance model with respect to the shape and appearance parameters, i.e.

$$\text{argmin}_{\mathbf{p},\boldsymbol{\lambda}} \|\mathbf{h}(\mathcal{W}(\mathbf{p})) - \bar{\mathbf{a}} - \mathbf{U}_A \boldsymbol{\lambda}\|^2 \tag{2}$$

In general, the IC optimization introduces an incremental warp that is applied on the residual term as

$$\text{argmin}_{\Delta\mathbf{p},\boldsymbol{\lambda}} \|\mathbf{h}(\mathcal{W}(\mathbf{p})) - \bar{\mathbf{a}}(\mathcal{W}(\Delta\mathbf{p})) - \mathbf{U}_A(\mathcal{W}(\Delta\mathbf{p}))\boldsymbol{\lambda}\|^2$$

This problem is solved by performing a first order Taylor expansion on the residual term with respect to the parameters increment $\Delta\mathbf{p}$ and composing the current warp with the incremental warp at each iteration as $\mathcal{W}(\mathbf{p}) \leftarrow \mathcal{W}(\mathbf{p}) \circ \mathcal{W}(\Delta\mathbf{p})^{-1}$. The linearization is

$$\bar{\mathbf{a}}(\mathcal{W}(\Delta\mathbf{p})) + \mathbf{U}_A(\mathcal{W}(\Delta\mathbf{p}))\boldsymbol{\lambda} \approx \bar{\mathbf{a}} + \mathbf{U}_A\boldsymbol{\lambda} + \mathbf{J}|_{\mathbf{p}=\mathbf{0}}\Delta\mathbf{p}$$

where $\mathbf{J}|_{\mathbf{p}=\mathbf{0}} = \nabla(\bar{\mathbf{a}} + \mathbf{U}_A\boldsymbol{\lambda}) \left.\frac{\partial \mathcal{W}}{\partial \mathbf{p}}\right|_{\mathbf{p}=\mathbf{0}}$ is the Jacobian. Note that the appearance model is based on the HOG representation of Eq. 1. Hence, in the partial derivative of the Jacobian, we make the assumption that $\frac{\partial \mathcal{H}}{\partial \mathbf{t}} \nabla\mathbf{t} \approx \nabla\mathcal{H}(\mathbf{t})$, which means that we neglect the partial derivative of $\mathcal{H}$ and deal with $\mathcal{H}(\mathbf{t})$ as a multichannel image. In this work, we use the Alternating and Project-Out IC algorithms.

Alternating: The AIC algorithm, proposed in [5], deals with the problem of Eq. 2, by solving two separate minimization problems, one for the shape and one for the appearance optimal parameters, in an alternating manner. The two cost functions are

$$\begin{cases} \text{argmin}_{\Delta\mathbf{p}} \|\mathbf{h}(\mathcal{W}(\mathbf{p})) - \mathbf{a}_{\boldsymbol{\lambda}}(\mathcal{W}(\Delta\mathbf{p}))\|^2_{\mathbf{I}-\mathbf{U}_A\mathbf{U}_A^T} \\ \text{argmin}_{\Delta\boldsymbol{\lambda}} \|\mathbf{h}(\mathcal{W}(\mathbf{p})) - \mathbf{a}_{\boldsymbol{\lambda}+\Delta\boldsymbol{\lambda}}(\mathcal{W}(\Delta\mathbf{p}))\|^2 \end{cases} \tag{3}$$

The minimization in every iteration is achieved by first using a fixed estimate of $\boldsymbol{\lambda}$ to compute the current estimate of $\Delta\mathbf{p}$ and then using the fixed estimate of $\mathbf{p}$ to compute the increment $\Delta\boldsymbol{\lambda}$. More specifically, given the current estimate of $\boldsymbol{\lambda}$, the shape parameters increment is computed from the first cost function using the orthogonal complement of the appearance subspace $\hat{\mathbf{U}}_A = \mathbf{I} - \mathbf{U}_A\mathbf{U}_A^T$ as

$$\Delta\mathbf{p} = \mathbf{H}^{-1}\mathbf{J}_{AIC}^T[\mathbf{h}(\mathcal{W}(\mathbf{p})) - \bar{\mathbf{a}} - \mathbf{U}_A\boldsymbol{\lambda}]$$

where $\mathbf{J}_{AIC} = \hat{\mathbf{U}}_A[\mathbf{J}_{\bar{\mathbf{a}}}|_{\mathbf{p}=\mathbf{0}} + \sum_{i=1}^{N_A} \lambda_i \mathbf{J}_{\mathbf{u}_i}|_{\mathbf{p}=\mathbf{0}}]$ and $\mathbf{H}^{-1} = \mathbf{J}_{AIC}^T\mathbf{J}_{AIC}$. Then, given the current estimate of the parameters $\mathbf{p}$, AIC computes the optimal appearance parameters as the least-squares solution of the second cost function of Eq. 3, thus

$$\Delta\boldsymbol{\lambda} = \mathbf{U}_A^T[\mathbf{h}(\mathcal{W}(\mathbf{p})) - \bar{\mathbf{a}}(\mathcal{W}(\Delta\mathbf{p})) - \mathbf{U}_A(\mathcal{W}(\Delta\mathbf{p}))\boldsymbol{\lambda}]$$

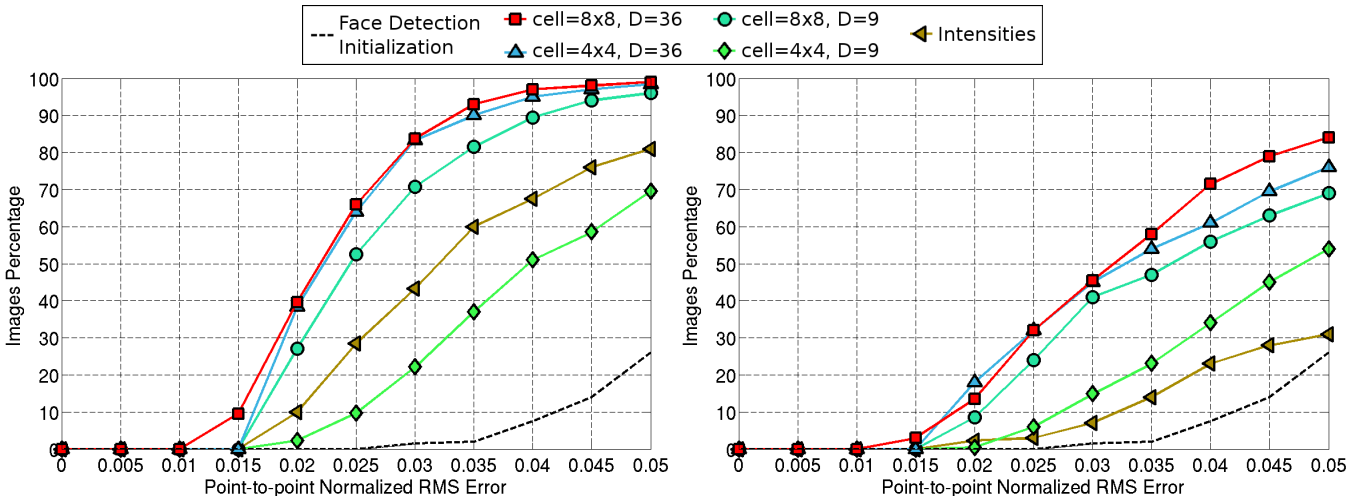

(a) Alternating IC (a) Project-Out IC

Fig. 2. Experimental results on the LFPW testing database evaluated on 68 points mask. We use various values for the HOG parameters ($N_{cell} \in \{4, 8\}$, $N_{block} \in \{1, 2\}$) and also compare with the intenisities-based AAMs using both the Alternating and Project-Out algorithms.

This alternating optimization is repeated at each iteration. The appearance parameters are updated in an additive mode, i.e. $\boldsymbol{\lambda} \leftarrow \boldsymbol{\lambda} + \Delta\boldsymbol{\lambda}$. Although the individual Jacobians $\mathbf{J}_{\mathbf{u}_i}|_{\mathbf{p}=\mathbf{0}}$, $\forall i = 1, \ldots, N_A$ and $\mathbf{J}_{\bar{\mathbf{a}}}|_{\mathbf{p}=\mathbf{0}}$ can be precomputed, the total Jacobian $\mathbf{J}_{AIC}$ and the Hessian need to be evaluated at each iteration. Following the Hessian matrix computation technique proposed in [5], which improves the cost from $\mathcal{O}(N_S^2 L_A)$ to $\mathcal{O}(N_S^2 N_A^2)$ (usually $L_A > N_A^2$), the total cost at each iteration is $\mathcal{O}(N_S^2 N_A^2 + (N_S + N_A)L_A + N_S^3)$.

Project-Out: The POIC algorithm [4] decouples shape and appearance by solving Eq. 2 in the subspace that is orthogonal to the appearance variation. This is achieved by "projecting-out" the appearance variation, thus, similar to the first problem of Eq. 3, the solution is computed based on the orthogonal complement of the appearance subspace $\hat{\mathbf{U}}_A = \mathbf{I} - \mathbf{U}_A \mathbf{U}_A^T$. The difference with the AIC case is that there is not an extra step for optimizing with respect to the appearance parameters. The cost function of Eq. 2 takes the form

$$\text{argmin}_{\Delta\mathbf{p}} \|\mathbf{h}(\mathcal{W}(\mathbf{p})) - \bar{\mathbf{a}}(\mathcal{W}(\Delta\mathbf{p}))\|^2_{\mathbf{I}-\mathbf{U}_A\mathbf{U}_A^T} \quad (4)$$

and the first-order Taylor expansion is $\bar{\mathbf{a}}(\mathcal{W}(\Delta\mathbf{p})) \approx \bar{\mathbf{a}} + \mathbf{J}_{\bar{\mathbf{a}}}|_{\mathbf{p}=\mathbf{0}}\Delta\mathbf{p}$. The shape parameters increment is computed as

$$\Delta\mathbf{p} = \mathbf{H}^{-1}\mathbf{J}_{POIC}^T[\mathbf{h}(\mathcal{W}(\mathbf{p})) - \bar{\mathbf{a}}]$$

where $\mathbf{H}^{-1} = \mathbf{J}_{POIC}^T\mathbf{J}_{POIC}$ and $\mathbf{J}_{POIC} = \hat{\mathbf{U}}_A\mathbf{J}_{\bar{\mathbf{a}}}|_{\mathbf{p}=\mathbf{0}}$. The appearance parameters can be retrieved at the end of the iterative operation as $\boldsymbol{\lambda} = \mathbf{U}_A^T[\mathbf{h}(\mathcal{W}(\mathbf{p})) - \bar{\mathbf{a}}]$ in order to reconstruct the appearance vector. The POIC algorithm is faster than AIC, with computational complexity of $\mathcal{O}(N_S L_A + N_S^2)$, because the Jacobian, the Hessian matrix and its inverse are constant and can be precomputed.

4. EXPERIMENTAL RESULTS

In this section we carry out experiments on three challenging in-the-wild databases, which consist of images downloaded from the web that are captured in totally unconstrained conditions and exhibit large variations in pose, identity, illumination, expressions, occlusion and resolution. We train our HOG-AAM model on 811 training images of the LFPW [17] training set (the rest of the database's images URLs are invalid), keeping $N_S = 15$ eigenshapes and $N_A = 100$ eigentextures. We acquired the groundtruth annotations of 68 points from the 300 Faces In-The-Wild Challenge [18]. The fitting process is initialized by computing the face's bounding box using the Cascade Deformable Part Models face detector [19] and then estimating the appropriate global similarity transform that fits the mean shape within the bounding box bounds. Note that this initial similarity transform only involves a translation and scaling component and not any in-plane rotation. The accuracy of the fitting results is measured by the point-to-point RMS error normalized by the face size, as proposed in [20]. Denoting the fitted and the groundtruth shapes as $\mathbf{s}^f$ and $\mathbf{s}^g$ respectively and the face's size as $s_f = (\max x_i^g - \min x_i^g + \max y_i^g - \min y_i^g)/2$, then the error is expressed as RMSE $= \frac{\sum_{i=1}^{L} \sqrt{(x_i^f - x_i^g)^2 + (y_i^f - y_i^g)^2}}{s_f L_S}$.

Comparison between HOG Features Variants: Herein, we conduct an experiment to compare the performance of HOG AAMs for various combinations of the parameters values presented in Sec. 2. Specifically, we use cell size values of $N_{cell} \in \{4, 8\}$ and experiment with the employment of block normalization by setting $N_{block} \in \{1, 2\}$, which results in HOG images with $D \in \{9, 36\}$ number of channels. Moreover, we compare our HOG AAMs with the intensities-based AAMs. The experiment is performed on the 224 images of the LFPW testing set. The results are demonstrated in Fig. 2 in the form of Cumulative Error Distribution (CED). This experiment proves that the block normalization has a great impact on the fitting result, while the reduction of the cell size provokes a small decline on the fitting accuracy. Additionally, HOG AAMs clearly outperform the intensities-based AAMs. Especially, in the case of HOGs wich $N_{cell} = 8$ and block normalization ($D = 36$), the difference is approximately 30% and 40% in the cases of RMSE less than 0.02 and 0.03 respectively.

Comparison with State-Of-The-Art Methods: In this cross-database experiment, we compare the performance of our HOG AAMs against two recently proposed state-of-the-art facial trackers: Supervised Descent Method (SDM) [7] and Robust Discriminative Response Map Fitting (DRMF) for CLMs [21]. We utilize the implementations provided online by their authors with their pre-trained models. Note that both these methods are trained on thousands of images, much more than the 811 images used to train our AAMs.

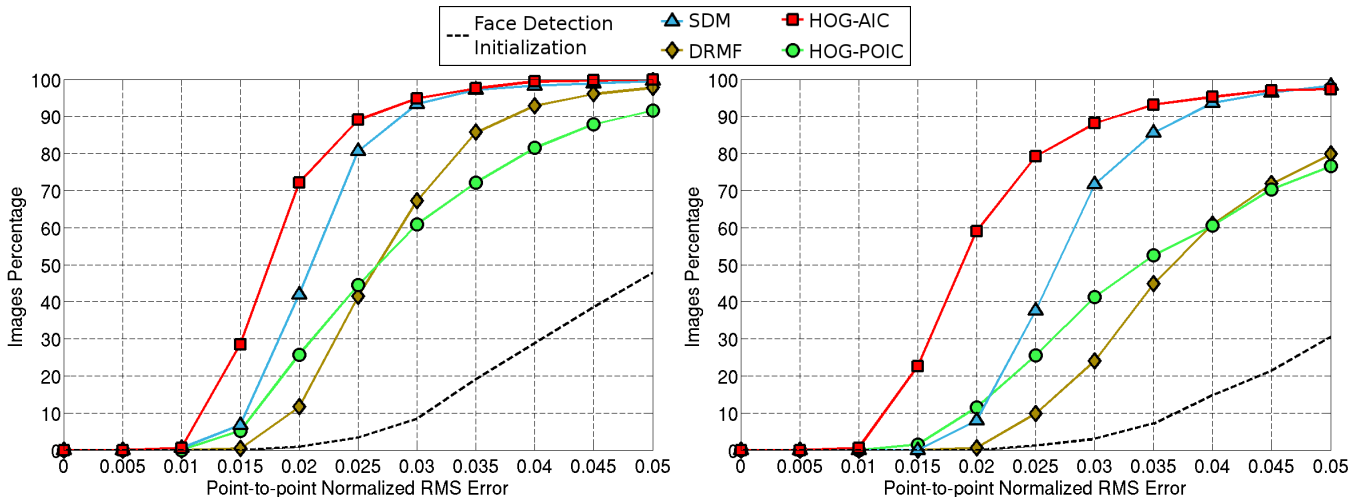

(a) Helen Database (a) AFW Database

Fig. 3. Comparison of HOG AAMs with state-of-the-art methods (SDM [7], DRMF [21]) on Helen and AFW databases, evaluated on 49 points mask.

Fig. 4. Fitting examples using HOG-AIC on AFW and Helen images. *Top row:* Initialization from bounding box. *Bottom row:* Fitting result.

Method	*Helen*		*AFW*	
	mean	*std*	*mean*	*std*
HOG-AIC	**0.0184**	**0.0058**	**0.0215**	**0.0129**
SDM	0.0216	0.0059	0.0484	0.5002
HOG-POIC	0.0300	0.0140	0.0395	0.0212
DRMF	0.0280	0.0086	0.0517	0.0611
Face Detection	0.0532	0.0196	0.0635	0.0227

Table 1. Statistics (mean and standard deviation) of Figure 3 results.

We use the best performing HOG parameters from the previous experiment, thus we set the cell size at 8×8 pixels and the block size at 2×2 cells, ending up with HOG feature images of $D = 36$ channels. The testing is performed on the very challenging in-the-wild databases of AFW [20] and Helen [22] which consist of 337 and 330 testing images respectively. Similar to the LFPW database, we acquired the groundtruth annotations from [18]. In this experiment we report results evaluated on 49 points shape mask instead of the 68 points of the previous one. This is because the SDM framework [7] returns only these 49 points, which occur by removing the 17 points of the boundary (jaw) and the 2 points from the mouth's corners. Thus, this evaluation framework emphasizes on the internal facial areas (eyebrows, eyes, nose, mouth).

Figure 3 demonstrates the results on Helen and AFW databases and Table 1 reports the corresponding statistics (mean and standard deviation of the errors). The results indicate that HOG-AIC significantly outperforms both DRMF and SDM and even the less accurate HOG-POIC performs better than DRMF. Moreover, note that because the AFW database is more challenging than the Helen one, the face detection initialization is worse and the performance of all methods greatly decreases, apart from the HOG-AIC model that preserves its accurate and robust behaviour. Figure 4 shows some indicative fitting results along with the initializations. Given the in-the-wild nature of the testing databases and the small number of training images, we believe that this performance is remarkable.

5. CONCLUSIONS

In this paper we present a formulation of AAMs Inverse Compositional fitting algorithm that employs dense HOG feature descriptors. This allows us to take advantage of the strengths and descriptive qualities of HOGs in order to achieve efficient, robust and accurate performance for the task of face fitting. Our experiments on challenging in-the-wild databases show that the HOG AAMs have the ability to generalize well to unseen faces and demonstrate invariance to expression, pose and lighting variations. Finally, we show that our method outperforms discriminative state-of-the-art methods trained on thousands of images.

6. REFERENCES

[1] Timothy Cootes, Gareth Edwards, and Christopher Taylor, "Active appearance models," *IEEE Trans. on Pattern Analysis and Machine Intelligence (TPAMI)*, vol. 23, no. 6, pp. 681–685, 2001.

[2] Michael Kass, Andrew Witkin, and Demetri Terzopoulos, "Snakes: Active contour models," *Int'l Journal of Computer Vision (IJCV)*, vol. 1, no. 4, pp. 321–331, 1988.

[3] Timothy Cootes, Christopher Taylor, David Cooper, and Jim Graham, "Active shape models-their training and application," *Computer Vision and Image Understanding*, vol. 61, no. 1, pp. 38–59, 1995.

[4] Iain Matthews and Simon Baker, "Active appearance models revisited," *Int'l Journal of Computer Vision (IJCV)*, vol. 60, no. 2, pp. 135–164, 2004.

[5] George Papandreou and Petros Maragos, "Adaptive and constrained algorithms for inverse compositional active appearance model fitting," in *IEEE Proc. of Computer Vision and Pattern Recognition (CVPR)*, 2008.

[6] G. Tzimiropoulos, J. Alabort-Medina, S. Zafeiriou, and M. Pantic, "Generic active appearance models revisited," in *Asian Conf. on Computer Vision (ACCV)*, 2012.

[7] Xuehan Xiong and Fernando De la Torre, "Supervised descent method and its applications to face alignment," in *IEEE Proc. of Computer Vision and Pattern Recognition (CVPR)*, 2013.

[8] Ce Liu, Jenny Yuen, Antonio Torralba, Josef Sivic, and William T Freeman, "Sift flow: dense correspondence across different scenes," in *European Conf. on Computer Vision (ECCV)*. 2008.

[9] Timothy Cootes and Christopher Taylor, "On representing edge structure for model matching," in *IEEE Proc. of Computer Vision and Pattern Recognition (CVPR)*, 2001.

[10] Mikkel B Stegmann and Rasmus Larsen, "Multi-band modelling of appearance," *Image and Vision Computing*, vol. 21, no. 1, pp. 61–67, 2003.

[11] Simon Lucey, Sridha Sridharan, Rajitha Navarathna, and Ahmed Bilal Ashraf, "Fourier lucas-kanade algorithm," *IEEE Trans. on Pattern Analysis and Machine Intelligence (TPAMI)*, vol. 35, no. 6, pp. 1383–1396, 2013.

[12] Ya Su, Dacheng Tao, Xuelong Li, and Xinbo Gao, "Texture representation in aam using gabor wavelet and local binary patterns," in *IEEE Int'l Conf. on Systems, Man and Cybernetics (SMC)*, 2009.

[13] Xinbo Gao, Ya Su, Xuelong Li, and Dacheng Tao, "Gabor texture in active appearance models," *Journal of Neurocomputing*, vol. 72, no. 13, pp. 3174–3181, 2009.

[14] Yongxin Ge, Dan Yang, Jiwen Lu, Bo Li, and Xiaohong Zhang, "Active appearance models using statistical characteristics of gabor based texture representation," in *Journal of Visual Communication and Image Representation*, 2013.

[15] Navneet Dalal and Bill Triggs, "Histograms of oriented gradients for human detection," in *IEEE Proc. of Computer Vision and Pattern Recognition (CVPR)*, 2005.

[16] Oswaldo Ludwig, David Delgado, Valter Gonçalves, and Urbano Nunes, "Trainable classifier-fusion schemes: an application to pedestrian detection," in *IEEE Int'l Conf. on Intelligent Transportation Systems (ITSC)*, 2009.

[17] Peter N Belhumeur, David W Jacobs, David J Kriegman, and Neeraj Kumar, "Localizing parts of faces using a consensus of exemplars," in *IEEE Proc. of Computer Vision and Pattern Recognition (CVPR)*, 2011.

[18] C. Sagonas, G. Tzimiropoulos, S. Zafeiriou, and M. Pantic, "300 faces in-the-wild challenge: The first facial landmark localization challenge," in *Proc. of IEEE Intl Conf. on Computer Vision (ICCV-W 2013), 300 Faces in-the-Wild Challenge (300-W)*, 2013.

[19] J. Orozco, B. Martinez, and M. Pantic, "Empirical analysis of cascade deformable models for multi-view face detection," in *IEEE Proc. of Int'l Conf. on Image Processing (ICIP)*, 2013.

[20] Xiangxin Zhu and Deva Ramanan, "Face detection, pose estimation, and landmark localization in the wild," in *IEEE Proc. of Computer Vision and Pattern Recognition (CVPR)*, 2012.

[21] Akshay Asthana, Stefanos Zafeiriou, Shiyang Cheng, and Maja Pantic, "Robust discriminative response map fitting with constrained local models," in *IEEE Proc. of Computer Vision and Pattern Recognition (CVPR)*, 2013.

[22] Vuong Le, Jonathan Brandt, Zhe Lin, Lubomir Bourdev, and Thomas S Huang, "Interactive facial feature localization," in *European Conf. on Computer Vision (ECCV)*. 2012.